FISEVIER

Contents lists available at ScienceDirect

# Science of the Total Environment

journal homepage: www.elsevier.com/locate/scitotenv



# Improved extraction efficiency of natural nanomaterials in soils to facilitate their characterization using a multimethod approach



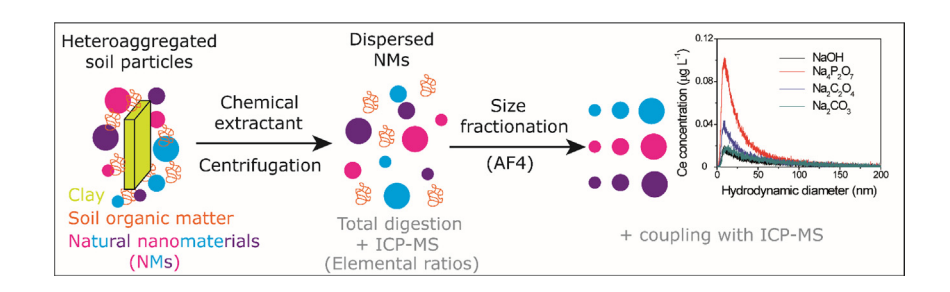
Frédéric Loosli a,b,\*, Zebang Yi a,c, Jingjing Wang a, Mohammed Baalousha a,\*\*

- a Center for Environmental Nanoscience and Risk, Department of Environmental Health Sciences, Arnold School of Public Health, University of South Carolina, SC 29208, USA
- <sup>b</sup> Centre for Microbiology and Environmental Systems Science, University of Vienna, 1090 Vienna, Austria
- <sup>c</sup> College of Earth Science, Guilin University of Technology, Guilin 541004, China

#### HIGHLIGHTS

- Efficient extraction of natural nanomaterials from complex environmental matrices
- Multimethod approach for characterization of natural nanomaterials from soils
- Sodium pyrophosphate to efficiently disperse nanomaterials from soil heteroaggregates
- Key nanomaterial properties to discriminate engineered from natural nanomaterials in soils

#### GRAPHICAL ABSTRACT



#### ARTICLE INFO

Article history:
Received 2 March 2019
Received in revised form 19 April 2019
Accepted 20 April 2019
Available online 24 April 2019

Editor: Damia Barcelo

Keywords:
Natural nanomaterial characterization
Nanomaterial extraction
Nanomaterial dispersion
Field flow fractionation
Sodium pyrophosphate

#### ABSTRACT

Characterization of natural nanomaterial (NNM) physicochemical properties - such as size, size distribution, elemental composition and elemental ratios - is often hindered by lack of methods to disperse NNMs from environmental samples. This study evaluates the effect of extractant composition, pH, and ionic strength on soil NNM extraction in term of recovery and release of primary particles/small aggregate sizes (i.e., <200 nm). The extracted NNMs were characterized for hydrodynamic diameter and zeta potential by dynamic light scattering and laser Doppler electrophoresis, natural organic matter desorption by UV–Vis spectroscopy, element composition by inductively coupled plasma-mass spectroscopy (ICP-MS), size based elemental distribution by field flow fractionation coupled to ICP-MS, and morphology by transmission electron microscopy. The extracted NNM concentrations increased following the order of NaOH  $\leq$  Na<sub>2</sub>CO<sub>3</sub> < Na<sub>2</sub>C<sub>2</sub>O<sub>4</sub> < Na<sub>4</sub>P<sub>2</sub>O<sub>7</sub>. Na<sub>4</sub>P<sub>2</sub>O<sub>7</sub> was the most efficient extractant and results in 2-12 folds higher NNM extraction than other extractants. The Na<sub>4</sub>P<sub>2</sub>O<sub>7</sub> extracted NNMs exhibited narrower size distribution with smaller modal size relative to NaOH, Na2CO3, Na2C2O4 extracted NNMs. Thus,  $Na_4P_2O_7$  enhances the extraction of primary NNMs and/or smaller NNM aggregates (i.e., size <200 nm).  $Na_4P_2O_7$ promote soil microaggregates breakup and release of NNMs by reducing free multivalent cation concentration in soil pore water by forming metal-phosphate complexes and by enhancing NNM surface charge via phosphate sorption on NNM surfaces, Additionally, the extracted NNM concentrations increased with the increase in extractant concentration and pH, except at 100 mM where the high ionic strength might have induced NNM aggregation. The improved NNM-extraction will improve the overall understanding of the physicochemical properties of NNMs in environmental systems. This study presents the key properties of NNMs that can be used as background information to differentiate engineered nanomaterials (ENMs) from NNMs in complex environmental media.

© 2019 Elsevier B.V. All rights reserved.

 $\textit{E-mail addresses:} \ looslifred@gmail.com\ (F.\ Loosli), \ mbaalous@mailbox.sc.edu\ (M.\ Baalousha). \ and \ a$ 

<sup>\*</sup> Correspondence to: F. Loosli, Centre for Microbiology and Environmental Systems Science, University of Vienna, 1090 Vienna, Austria.

<sup>\*\*</sup> Corresponding author.

#### 1. Introduction

Soil is an important reservoir of inorganic and organic natural particles such as clay minerals, metal oxides, and humic substances (Gieseking, 1975a, 1975b). Natural nanomaterials (NNMs) are important constituents of soils, because they are involved in numerous fundamental biogeochemical processes such as water regulation, element cycling and bioavailability through sorption, retention and transport of nutrients, natural organic matter (NOM) and organic/inorganic contaminants (McCarthy and Zachara, 1989; Theng and Yuan, 2008). These processes are strongly influenced by NNM physicochemical properties (Nowack and Bucheli, 2007). Soils are also expected to become a reservoir for anthropogenic materials (i.e., incidental and engineered nanomaterials, ENMs) (Mueller and Nowack, 2008) mainly due to the application of wastewater sludge as fertilizer but also from intentional and accidental releases (El Hadri et al., 2018; Klaine et al., 2008). ENMs are currently produced in large volumes (Piccinno et al., 2012) and are used in many novel applications and consumer products due to their very unique physico-chemical properties (i.e., optical, mechanical, narrow monomial size distribution, specific surface coating etc.) (Chen and Mao, 2007; Lu et al., 2007; Stark et al., 2015). ENMs are thus prompt to enter environmental compartments including soil (Keller and Lazareva, 2014; Song et al., 2017), where they may pose environmental and human health concerns. ENM risk assessment entails ENM exposure characterization and thus quantification and characterization of ENM physicochemical properties size, size distribution, elemental composition and ratios, morphology. Nonetheless, quantification and characterization of ENMs in complex environmental matrices remain a significant challenge in environmental nanoscience and engineering (Montano et al., 2014; Wagner et al., 2014) due to (i) the low concentration of ENMs (several order of magnitude) relative to NNMs (Praetorius et al., 2017), (ii) the similarity in the chemical composition between NNMs and ENMs (Gondikas et al., 2018; von der Kammer et al., 2012), and (iii) the tendency of NNMs and ENMs to heteroaggregates in the natural environment (Praetorius et al., 2014; Wang et al., 2015). Thus, understanding the physicochemical properties (e.g., size, size distribution, elemental composition and ratios) of NNMs is essential to develop approaches to distinguish ENMs from NNMs based on differences in their physicochemical properties.

Natural organic matters (NOM) strongly associate with NMs and tend to form large heteroaggregates through organo-mineral interactions (Buffle et al., 1998; Cornelis et al., 2014). For electrostatically stabilized NM, which is the most prevalent NM stabilization mechanism, heteroaggregation/disaggregation is mainly controlled by NM surface charge. The latter is largely determined by the media physicochemical properties such as ionic strength, counter ion concentration and valency, pH, and concentration, and properties of NOM (Baalousha, 2009; Loosli et al., 2015; Philippe and Schaumann, 2014). Whereas, higher ionic strength promotes NM aggregation via surface charge screening, higher pH and NOM concentration promotes NM colloidal stability by enhancing NM surface charge. Nonetheless, high concentrations of both NOM and multivalent counterions promote NM aggregation via bridging mechanism (Chen et al., 2006, 2007). Thus, scavenging multivalent cations and promoting NOM desorption/dissolution may enhance NM surface charge, and thus electrostatic repulsions between NMs, and ultimately favor disaggregation processes (Loosli et al., 2018). Extraction of NNMs from soils usually consists of a combination of chemical treatment, i.e. dispersion of soils into a liquid, and a physical treatment, e.g. sonication, followed by size separation by centrifugation or filtration (Bakshi et al., 2014; Li et al., 2012; Tang et al., 2009). NNM Extraction efficiency depends on the experimental conditions, i.e., pH, ionic strength, sonication time and on the chemical proprieties of the extractant (Pronk et al., 2011). Alkaline condition enhances soil organic matter (SOM) solubilization/desorption and may favor disaggregation process of organo-mineral heteroaggregates. Nevertheless, soil extraction in NaOH is not sufficient to disperse NNMs as primary particle, because forces applied during sonication are not sufficient to break organo-mineral heteroaggregates (Regelink et al., 2013a, 2013b). To enhance NNM extraction efficiency, complexation agents, e.g. Na<sub>2</sub>C<sub>2</sub>O<sub>4</sub>, EDTA, Na<sub>4</sub>P<sub>2</sub>O<sub>7</sub>, are used to sequestre multivalent cations released from clays during extraction processes due to cation exchange and mineral delamination (Liu et al., 2015; Novikova et al., 2016). Such extractants prevent specific adsorption of multivalent cations onto particles which is known to strongly destabilize particles (Jolivet, 2000) and were effective to extract NNMs in soils (Calabi-Floody et al., 2011). Phosphate based extractant are also shown to adsorb specifically on colloids and modify their surface charge and facilitate disaggregation processes (Jeanroy and Guillet, 1981).

The aggregation of NNMs in soils complicates primary NNM characterization. Thus, in order to quantify and characterize NNMs in soils, it is necessary to extract/disperse primary NNMs and/or small aggregates (*i.e.* size <200 nm) from soil microaggregates (*i.e.* size >1000 nm) (Baalousha et al., 2005; Montano et al., 2014; Regelink et al., 2013a). Thus, the aims of this study are to: (i) evaluate the effect extractant chemical properties, concentration and pH on the extraction efficiency of NNMs, and (ii) characterize the properties – size distribution and elemental composition and ratio – of the extracted soil NNMs using a multimethod approach including dynamic light scattering, UV–Vis, flow-field flow fractionation coupled to inductively coupled plasmamass spectroscopy (AF4–ICP–MS), and transmission electron microscopy (TEM).

## 2. Material and methods

### 2.1. Soil sampling and geographic location

The topsoil sample used in this study was collected in Marion County which is situated in the coastal plain region of South Carolina, USA. The soil was characterized as Dothan series which consists of very deep and well drained soils. These series are formed from clay and loamy marine sediments. The soil sample was collected from the surface horizon 15 cm below the surface (A horizon) which consists mainly of sandy loam. The soil sample is characterized by brown color and weak fine granular structure (USDA, 2017). The soil was collected using a hand drill and preserved in polyethylene bag. Dry soils were sieved through a 10-mesh (2 mm) nylon sieve (Zhangxing instrument, China) to remove gravel and large debris. Then 100 g of the dry sieved soils were dispersed in 1 L of UPW, shook for 24 h and wet sieved through a 300-mesh (54 µm) nylon sieve (Zhangxing instrument, China) prior freeze drying (Freezone® 6, Labconco, USA).

#### 2.2. Chemicals

Ultrapure water (UPW) (PURELAB Option-Q, ELGA, UK) was used to prepare all solutions. Tetrasodium pyrophosphate (Na<sub>4</sub>P<sub>2</sub>O<sub>7</sub>, analytical grade, Alfa Aesar Japan), Sodium oxalate (Na<sub>2</sub>C<sub>2</sub>O<sub>4</sub>, analytical grade, Alfa Aesar, China), and Sodium carbonate (Na<sub>2</sub>CO<sub>3</sub>, ACS grade, BDH, USA) were used to extract NNMs from soil. 1 M sodium hydroxide (ACS grade, BDH, USA) and hydrochloric acid (Trace metal grade, Fisher Chemicals, Canada) were used to adjust the pH of soil suspensions. Nitric acid (Trace metal grade, Fisher Chemicals, Canada) was used at a 2% (v/v) to prepare ICP-MS calibration standards. Sodium nitrate (NaNO<sub>3</sub>, ACS grade, BDH, Canada), Sodium azide (NaN<sub>3</sub>, 99%, Fisher brand, USA), and FL-70 detergent (Fisher brand, USA) were used to prepare the AF4 carrier solution. Nitric acid (HNO<sub>3</sub>) and hydrofluoric acid (HF), and hydrochloric acid (HCl) were used to digest the extracted NNM suspensions and were all distilled from reagent grade acids. HNO<sub>3</sub> and HF were purified using a custom made sub-boiling perfluoroalkoxy alkanes (PFA) stills, and HCl was purified using a custom-made quartz double-still.

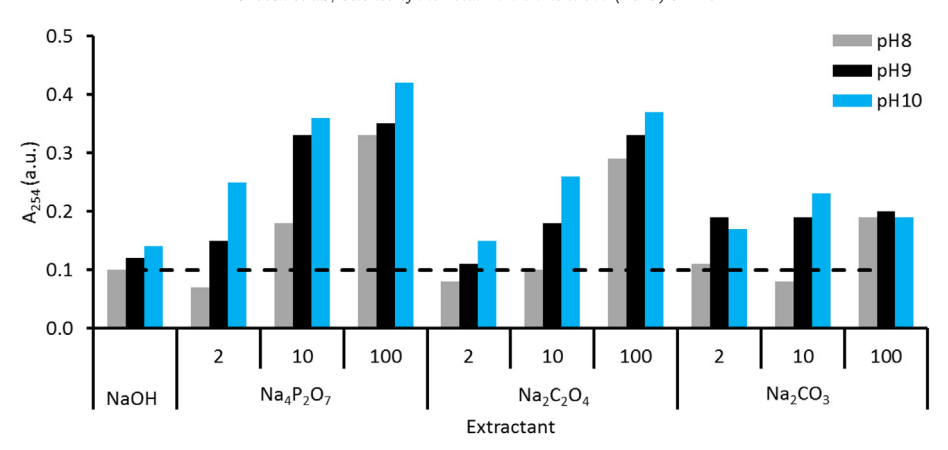


**Fig. 1.** UV–Vis absorbance at 254 nm ( $A_{254}$ ) of extracted NNM suspensions using different extractants at a range of pHs and concentrations. In the x-axis title, the numbers represent the concentration of the extractants (2, 10 and 100 mM). UV–Vis absorbance was measured on one soil sample for the 30 extraction conditions. The black dashed line correspond to the absorbance of the NNM suspension extracted with NaOH at pH 8 ( $A_{254} = 0.1$ ). The UV–Vis is reported in arbitrary units (a.u.).

#### 2.3. Soil NNM extraction

Soil NNMs were extracted using 2 mM, 10 mM and 100 mM  $Na_4P_2O_7$ ,  $Na_2C_2O_4$ , and  $Na_2CO_3$ . Soil NNMs were also extracted using NaOH as control extraction condition. 40 mL of extraction solution was added to 4 g of freeze dried soil in 50 mL polypropylene (PP)

centrifuge tube (Eppendorf, Mexico). The suspension was mixed at 40 rpm overnight with a tube rotator (Fisher brand, China) to enable wetting of the freeze-dried soil. The soil-extractant suspension pH was adjusted to pH 8, 9 and 10 and monitored throughout the experimental time using a pH meter (Mettler Toledo pH Electrode LE438, Switzerland). Suspensions were sonicated for 1 h in an ultrasonication

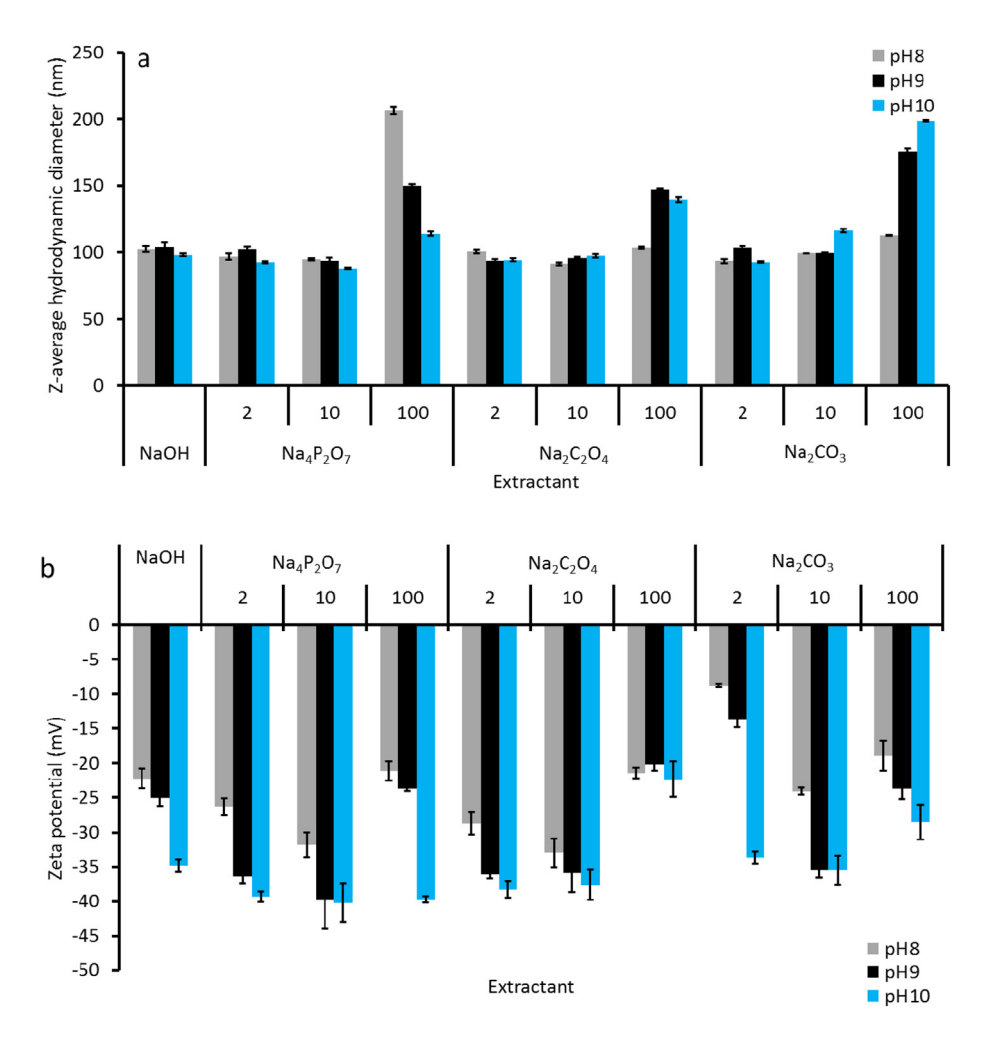


Fig. 2. (a) Z-average hydrodynamic diameter (Z-dh) and (b) zeta potential of extracted NNM suspensions as a function of extraction protocols.

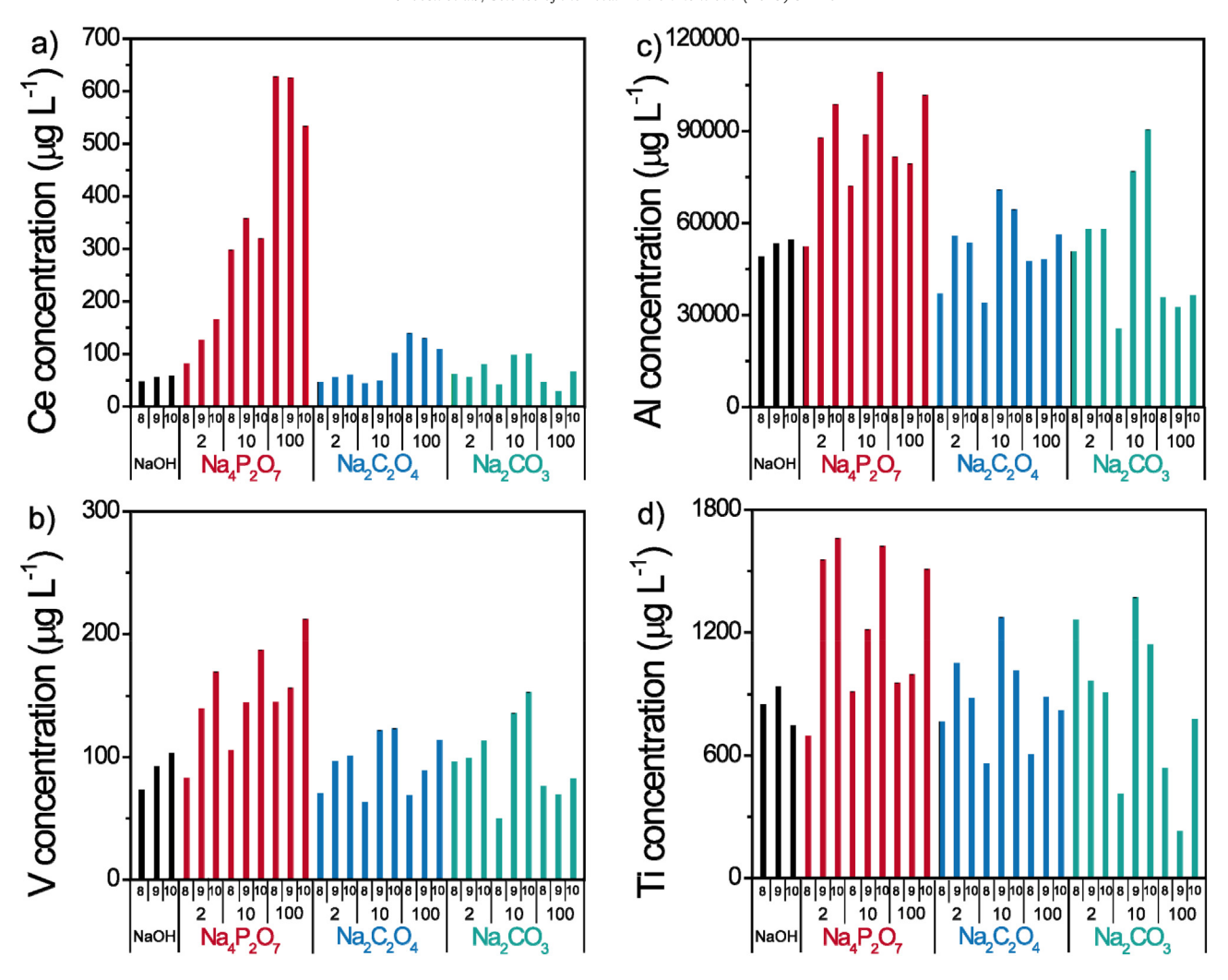


Fig. 3. Concentration of total digested soil nanosize fraction extracted by different dispersing agents at different concentration and pH conditions. In the x-axis title, the top numbers represent the pH (8, 9 and 10) and the second numbers represent the concentration of the extractants (2, 10 and 100 mM).

bath (Branson Model 2800, 40 kHz, USA). Samples were centrifuged (Eppendorf, 5810 R, Germany) for 90 min at 3100g to remove particles larger than 100 nm based on a particle density of 2.5 and Stokes' law

calculation assuming a spherical shape (Tang et al., 2009). Supernatants (25 mL) were carefully collected and stored in the dark at 4  $^{\circ}\text{C}$  until further analysis.

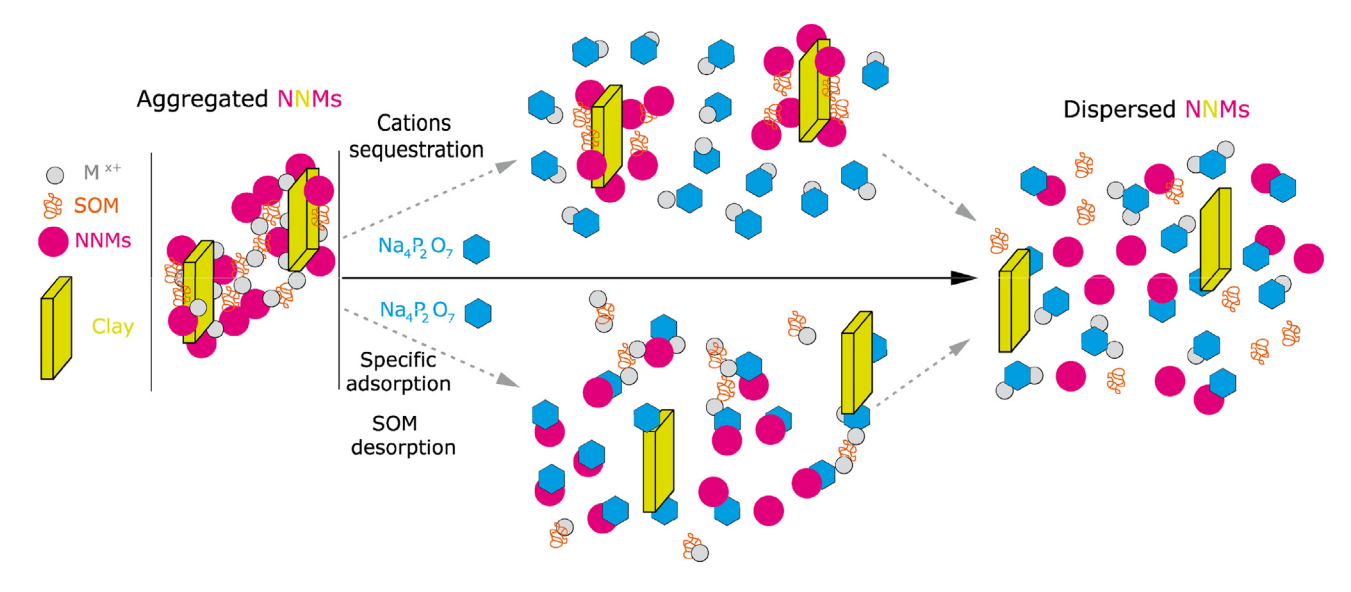


Fig. 4. Schematic representation of the main disaggregation mechanisms (cation sequestration/complexation and specific adsorption/SOM desorption) involved in dispersing NNM heteroaggregates in presence of  $Na_4P_2O_7$ . M  $^{\times +}$ , SOM and NNMs represent multivalent cations (x > 1), soil organic matter and natural nanomaterials, respectively.

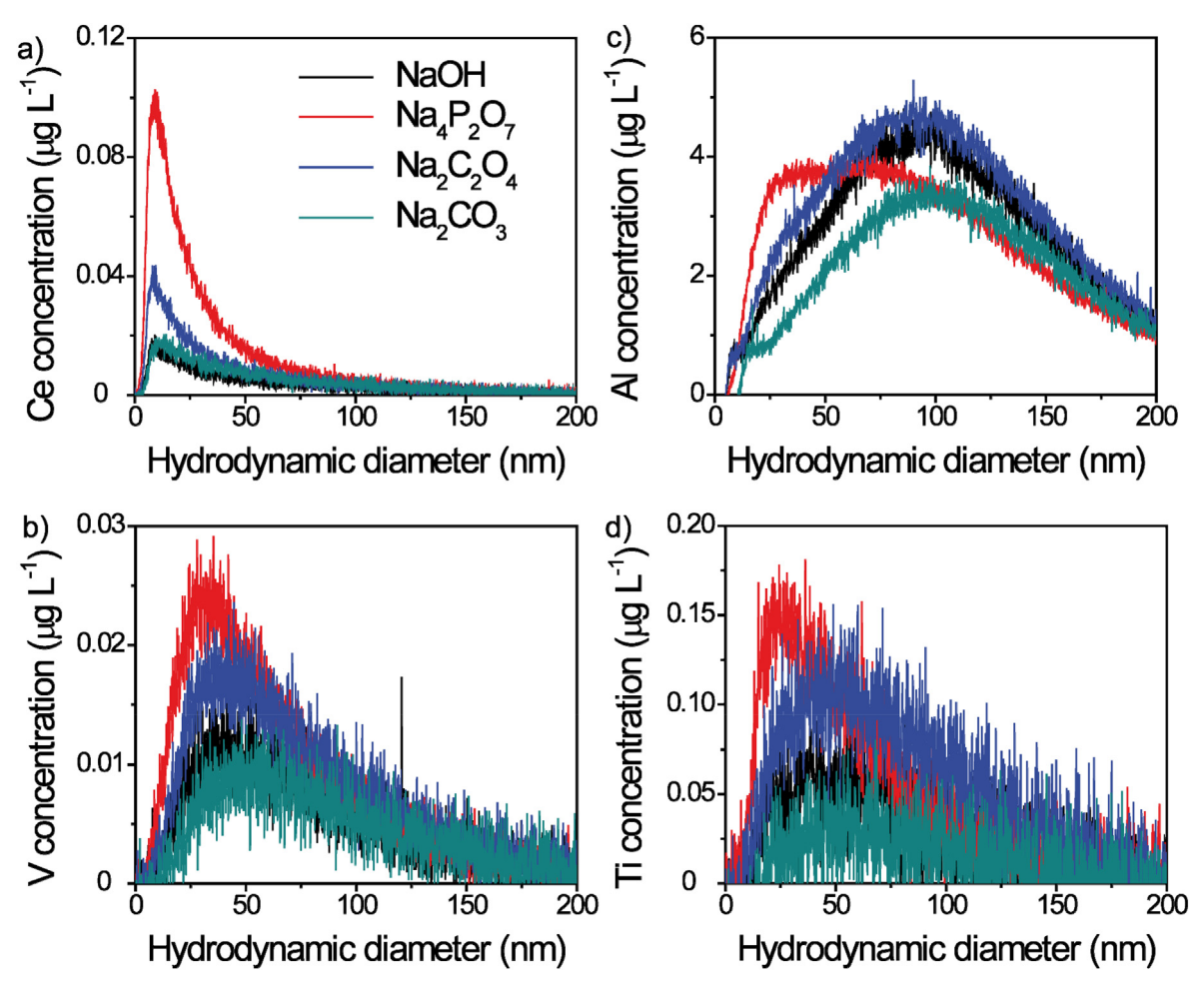


Fig. 5. Elemental concentration distributions of NNMs extracted by different chemical dispersant at pH 10 and 10 mM extractant concentration, a) Ce, b) V, c) Al and d) Ti.

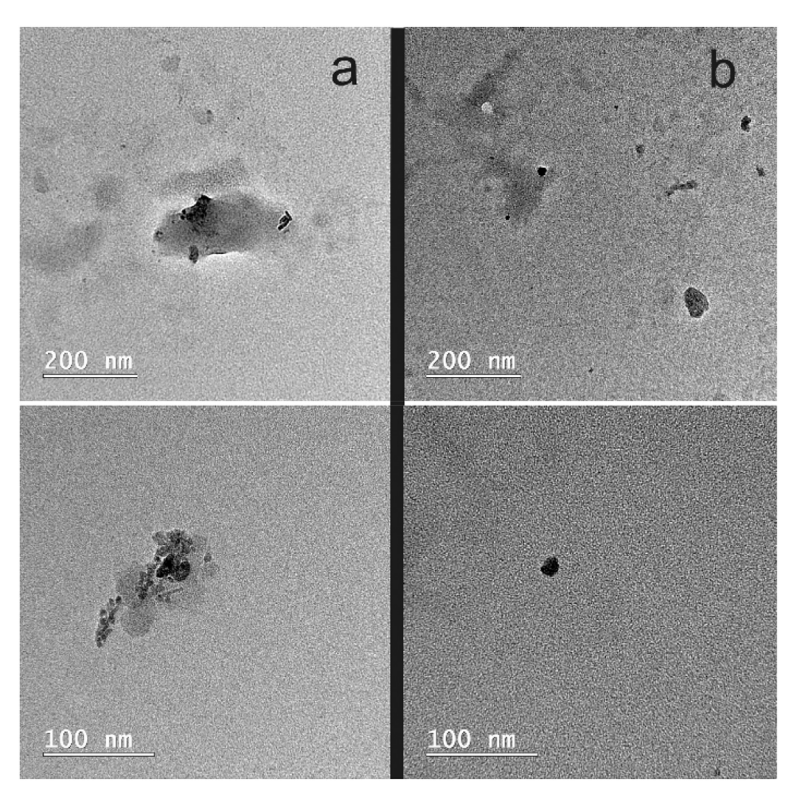


Fig. 6. TEM images of NNMs extracted by a) NaOH at pH 10 and b) 10 mM  $Na_4P_2O_7$  at pH 10.

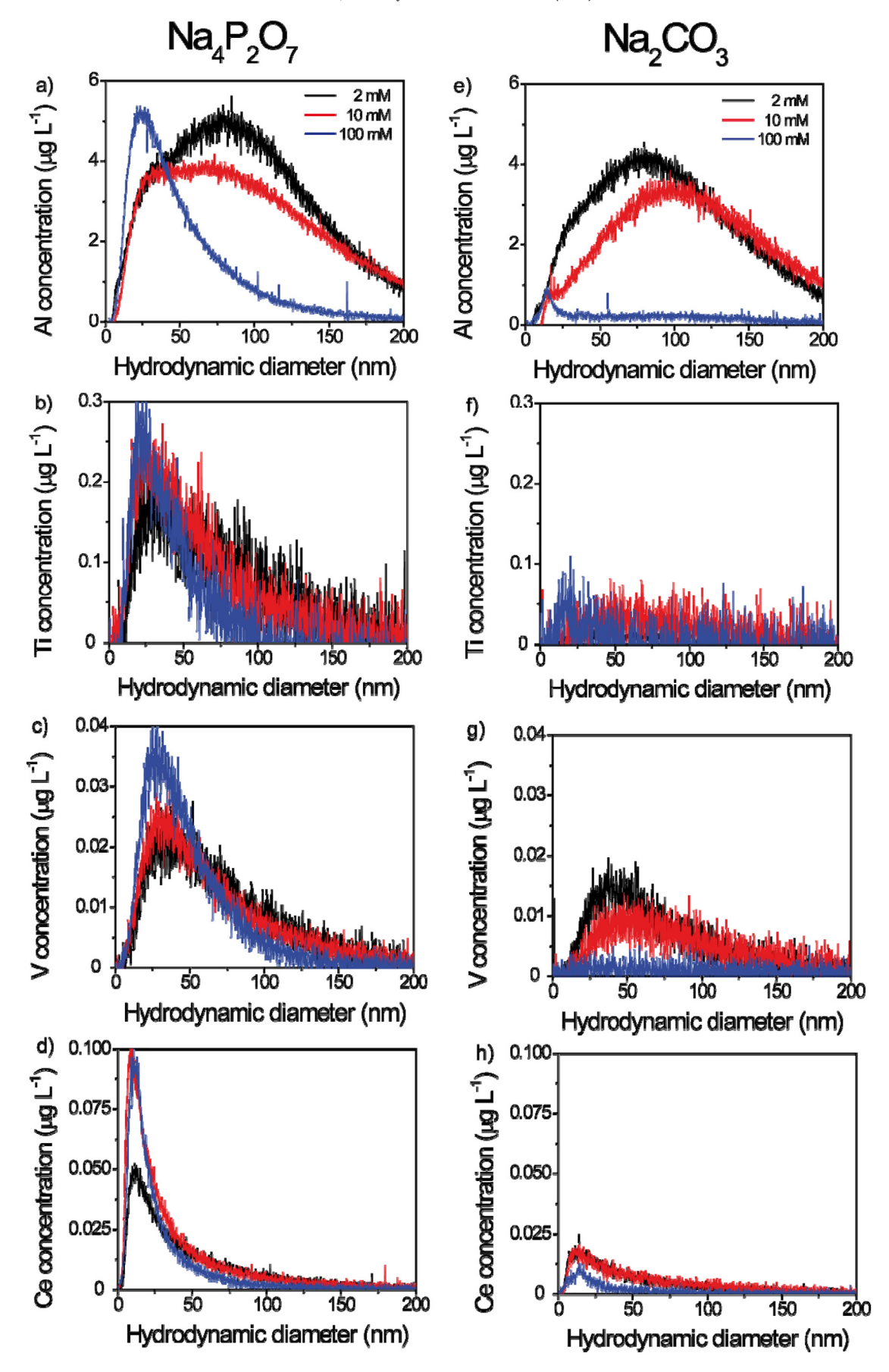


Fig. 7. Effect of  $Na_4P_2O_7$  and  $Na_2CO_3$  concentration on element concentration and size distribution at pH 10, a) Al, b) Ti, c) V and d) Ce. Black curves refer to 2 mM, red to 10 mN and blue to 100 mM.

# 2.4. General analysis on soil NNM suspensions

The NNMs z-average hydrodynamic diameter and zeta ( $\zeta$ ) potential were determined by dynamic light scattering (DLS) and laser Doppler electrophoresis (Malvern Nano ZS, USA) at 20 °C. The size distribution polydispersity index for all samples was below 0.4 and the Smoluchowski approximation (Makino and Ohshima, 2010; Murdock et al., 2007) was applied for  $\zeta$  potential determination. UV–Vis absorbance at a wavelength of 254 nm (A254) was recorded (UV 2600, Shimadzu Co., Japan) as a measure of NOM concentration in the extracted NNM suspensions. UV–Vis absorbance was measured on one soil sample for the 30 extraction conditions.

# 2.5. Soil NNM digestion and ICP-MS analysis

Soil NNM suspensions were digested in 15 mL Teflon vessels (Savillex, USA) on custom-made Teflon covered hotplates with double-HEPA filtered forced air in a metal-free HEPA filtered air clean lab. The digestion method was based on Gaudino et al. HF:HNO<sub>3</sub> (3:1) digestion of soils. Aliquots of NNM suspensions (5 mL) were weighted (Mettler Toledo, Excellence Plus, Switzerland) into Teflon vessels and dried down at 110 °C. The residue were treated for 2 h at 70 °C with 1 mL of H<sub>2</sub>O<sub>2</sub> 30% (Fisher Chemical, USA) to remove organic compounds. After H<sub>2</sub>O<sub>2</sub> evaporation, 2 mL of HF:HNO<sub>3</sub> (3:1) was added to the samples and allowed to digest at 110 °C for 24 h. Samples were dried down and treated twice with 1 mL HNO<sub>3</sub> to minimize the presence of insoluble fluorides. The samples were dissolved in 10 mL of 2% HNO<sub>3</sub>, sonicated for 5 min and heated at 50 °C for 2 h for complete dissolution. The solutions were transferred into 15 mL PP centrifuge tubes and preserved at 4 °C in the dark until further analysis. The samples were centrifuged for 5 min at 3100g prior ICP-MS analysis to remove any remaining refractory minerals.

Elemental concentrations of the digested NNM suspensions were determined on a high resolution ICP-MS (ELEMENT 2, Thermo Scientific, USA). Samples were injected to the ICP-MS using an APEXQ introduction system and a  $100~\mu L~min^{-1}$  PFA nebulizer. Amplifier gain calibration was performed daily. Baseline was determined by beam deflection. Typical runs consisted of 35–40 8.3 s integrations. The measured analytes were  $^{27}$ Al,  $^{47}$ Ti,  $^{51}$ V,  $^{90}$ Zr,  $^{93}$ Nb,  $^{139}$ La,  $^{140}$ Ce,  $^{178}$ Hf and  $^{181}$ Ta. ICP-MS calibration was performed using a mixture of two multielement standards, IV-ICPMS-71A (Inorganic Ventures, USA) and ICP-MS-68A-B (High-Purity Standards, USA).

# 2.6. AF4-ICP-MS analysis

NNM size-based elemental distribution of a subset of extracted NNMs was measured by asymmetric flow-field flow fractionation (AF4, Wyatt Eclipse® DualTec™, Germany) coupled to ICP-MS (Perkin Elmer NexION350D). The AF4 was equipped with 350 µm spacer and a 1 kDa polyether sulfonate membrane (Pall Corporation, USA). The AF4 carrier solution consisted of 10 mM NaNO<sub>3</sub> (VWR Analytical, BDH®, ACS, Canada), 0.01% NaN₃ (Fisher Bioreagents™, India), and 0.0125% FL-70 (Fisher Scientific, USA) in UPW. The detector and cross flows were 1.0 mL min<sup>-1</sup>. Sample injection volume was 5 µL and the focus time was 10 min. Polystyrene latex standards of 20, 40, 80, and 150 nm diameters (Nanosphere™, Thermo Scientific, USA) were used to calibrate particle size as a function of retention time.

ICP-MS was calibrated for the concentration range of  $0.1-100 \,\mu g \, L^{-1}$  using a mixture of two multi-element standards IV-ICPMS-71A and ICP-MS-68A-B. Samples were introduced to the ICP-MS using a T-junction to monitor internal standards (ICP Internal Element Group Calibration Standard, BDH Chemicals, USA) for quality control and to acidify (1% after mixing with the sample) the samples just prior introduction into the ICP-MS in order to avoid particle stability changes. In this configuration, the sample introduction flow rate was equal to 1.0 mL min<sup>-1</sup> and the acidified internal standard solution flow rate was 0.3 mL min<sup>-1</sup>. A

50 ms dwell time was applied for all the analytes. A 20 min 1% HNO<sub>3</sub>, 20 min 2% CH<sub>3</sub>OH and 10 min UPW rinses were applied field-off between each sample to clean the system and remove any deposited organic matter. Data were collected using Chromera 4.1.0.6386 software. Elemental recovery by AF4-ICP-MS was approximately 20–60% relative to the total elemental concentration measured following total digestion (Table S1).

#### 2.7. Transmission electron microscopy

Analysis of selected soil NNM suspensions extracted using NaOH, and Na<sub>4</sub>P<sub>2</sub>O<sub>7</sub> were performed using transmission electron microscope (TEM). TEM samples were prepared using drop deposition method according to the procedure described elsewhere (Prasad et al., 2015). Briefly, TEM grids were functionalized using a positively charged poly-L-lysine (1% w/v in water solution; Ted Pella, USA) to enhance the attachment of the negatively charged NNMs on the grid surface. 10 µL of poly-L-lysine were deposited on a 300 mesh Cu grid (Ted Pella, Pelco®, USA) for 20 min followed by rinsing three consecutive times in UPW water to remove excess poly-L-lysine. Subsequently, 20 µL of soil suspensions were deposited on the functionalized TEM grids for 15 min. The excess NNM suspension was then removed by immersing the TEM grid three times in UPW to avoid NNM aggregation during the drying process. The TEM grids were then left to dry for 12 h in a covered petri dish to avoid atmospheric particle deposition on the TEM grid. Samples were analyzed in a LaB<sub>6</sub> Jeol 2100 TEM, operated at 200 keV. Micrographs were acquired at different magnifications, ranging from 500× to 400,000×, to gather information about the NNM dispersion state (dispersed vs aggregated NNMs).

#### 3. Results and discussion

#### 3.1. General characteristic of the sample

The UV-Vis absorbance at  $\lambda_{254}$  (A<sub>254</sub>) is used here as a measure of the concentration of soil organic matter (SOM) released into solution during NNM extraction (Fig. 1) (Albrektienė et al., 2012; Buchanan et al., 2005). NaOH extracted NNMs have a relatively low A254 (ca. 0.1–0.14 a.u.), indicating that physical treatment (e.g., ultrasonication) is insufficient to desorb/release SOM, and thus insufficient to release NNMs from soil microaggregates (i.e. size >1000 nm). Similarly, the A<sub>254</sub> at 2 mM extractant concentration and pH 8 is relatively low (<0.1) for all extractants, indicating that these conditions are not optimal to releases SOM and to break up soil microaggregate. A<sub>254</sub> increased in the order of NaOH < Na<sub>2</sub>CO<sub>3</sub> < Na<sub>2</sub>C<sub>2</sub>O<sub>4</sub> < Na<sub>4</sub>P<sub>2</sub>O<sub>7</sub>, suggesting that  $Na_2C_2O_4$  and  $Na_4P_2O_7$  facilitates the desorption and release of SOM. Also, A<sub>254</sub> increases with increase in Na<sub>2</sub>C<sub>2</sub>O<sub>4</sub> and Na<sub>4</sub>P<sub>2</sub>O<sub>7</sub> concentrations and pH. However, A<sub>254</sub> did not show a specific trend with the increase in Na<sub>2</sub>CO<sub>3</sub> concentration. Nonetheless, the A<sub>254</sub> of Na<sub>2</sub>CO<sub>3</sub> extracted NNM suspensions was slightly higher at pH 9 and 10 compared to that at pH 8. For Na<sub>4</sub>P<sub>2</sub>O<sub>7</sub> extracted NNMs, the A<sub>254</sub> increased by 2.4 and 3.1 folds (e.g., to 0.29 and 0.36 a.u.) in 10 and 100 mM suspensions, respectively, compared to that of the NaOH extracted NNM suspensions. For Na<sub>2</sub>C<sub>2</sub>O<sub>4</sub> extracted NNMs, the A<sub>254</sub> increased by 1.5  $\pm$  0.4 and 2.8  $\pm$  0.2 folds (e.g., to 0.18 and 0.33 a.u.) at 10 and 100 mM Na<sub>2</sub>C<sub>2</sub>O<sub>4</sub>, respectively compared to that of the NaOH extracted NNM suspensions. Therefore, high pH (i.e. 9 and 10) in combination with chemical extractants facilitates the desorption and release of SOM from soil microaggregates as suggested in previous studies (Pronk et al., 2011).

The effect of extractants on the NNM size and zeta ( $\zeta$ ) potential are presented in Table S2 and Fig. 2. The z-average hydrodynamic diameter of NaOH extracted NNMs decreased slightly from 104 to 98 nm and the  $\zeta$  potential magnitude increased from 22.2 to 34.8 mV with the increase in pH from 8 to 10. Similarly, NNM z-average hydrodynamic diameter

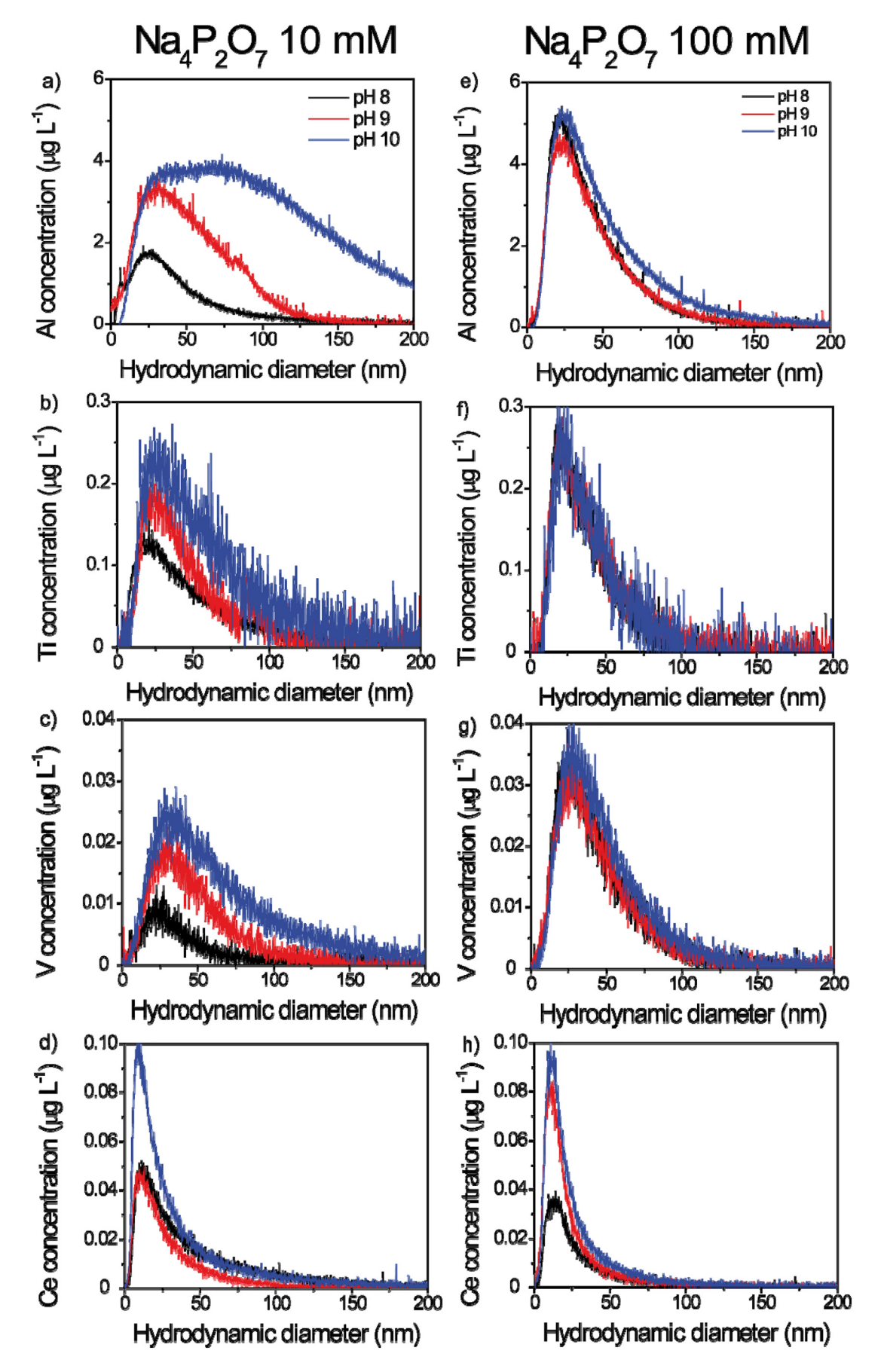


Fig. 8. Effect of pH on element concentration and size distribution for sodium pyrophosphate at 10 mM and 100 mM. a) Al, b) Ti, c) V and d) Ce. Black curves refer pH 8, red pH 9 and blue to pH 10.

decreased and ζ potential magnitude increased with the pH increase (pH 8 vs 10) for Na<sub>4</sub>P<sub>2</sub>O<sub>7</sub> extracted NNMs. For Na<sub>2</sub>CO<sub>3</sub> and Na<sub>2</sub>C<sub>2</sub>O<sub>4</sub> extracted NNMs, the z-average hydrodynamic diameter generally remained constant or increased with the increase in pH (pH 8 vs 10), whereas the  $\zeta$  potential magnitude increased with the increase in pH, except at 100 mM  $Na_2C_2O_4$ , where the  $\zeta$  potential did not change with the increase in pH. The higher  $\zeta$  potential magnitude of the extracted NNMs in the presence of chemical extractants than the corresponding ζ potential magnitude potential of NaOH extracted NNMs, at a given pH, indicates that extractant anions adsorb specifically on NNM surfaces. Several studies demonstrated the selective sorption of carbonate, phosphate, and oxalate anions on NNM surfaces (Jolivet, 2000) and that these anions replace SOM on NNM surfaces. This is in good agreement with the higher A<sub>254</sub> measured in NNM suspensions extracted using chemical extractants relative to those measured in NaOH extracted NNMs (Fig. 1).

At all pH conditions, Na<sub>2</sub>CO<sub>3</sub>, Na<sub>2</sub>C<sub>2</sub>O<sub>4</sub>, and Na<sub>4</sub>P<sub>2</sub>O<sub>7</sub> extracted NNMs exhibited a smaller z-average hydrodynamic diameter and higher  $\zeta$  potential magnitude at 2 and 10 mM extractant concentrations than at 100 mM extractant concentrations. The larger NNM z-average hydrodynamic diameter and lower  $\zeta$  potential magnitude at 100 mM extractant concentrations is likely due to NNM surface charge screening and aggregation at high ionic strength (Jiang et al., 2009; Suttiponparnit et al., 2011). Overall, the smallest NNM hydrodynamic size and highest  $\zeta$  potential magnitude were 88  $\pm$  1 nm and  $-40.2 \pm 2.8$  mV, respectively for 10 mM Na<sub>4</sub>P<sub>2</sub>O<sub>7</sub> extracted NNMs at pH 10, suggesting that these conditions (10 mM Na<sub>4</sub>P<sub>2</sub>O<sub>7</sub> at pH 10) are the most favorable conditions for the extraction of NNMs from soil.

These observations are in good agreement with NNM aggregation behavior, which is strongly influenced by particles surface charge. Several soil minerals and NNMs, such as Al- and Fe-oxides, have a point of zero charge (PZC) at pH > 8 (Fisher-Power and Cheng, 2018), and thus, they are positively charged in the pH range 4.5–7.5 of most soils which will lead the NNM heteroaggregation mediated by SOM and multivalent cations. Higher pHs (*i.e.*, above NNM PZC) enhance NNM and SOM negative surface charge by enhancing the dissociation of surface hydroxylic- and carboxylic-bearing functional groups (pKa ranging from 4 to 10, with functional groups with pKa ~9 being the most firmly bonded to soils (Shamrikova et al., 2006, 2007)).

It is worth noting here that the z-average hydrodynamic diameter was close to the size cut-off selected to extract NNMs; that is 100 nm. This is because the z-average hydrodynamic diameter measured by DLS is intensity weighted and is thus biased toward larger particles in polydispersed samples (Baalousha and Lead, 2012) because the intensity of the scattered light (I) is proportional to the particle diameter (d) to the power 6 (i.e., I  $\alpha$  d $^6$ ). Therefore, the hydrodynamic diameter of the extracted NNMs was measured by AF4-ICP-MS (see Section 3.3) in order to better understand the impact of extractants on NNM size distribution.

# 3.2. NNM extraction efficiency

The total concentrations of selected elements (Ce, Al, V and Ti) in the extracted NNM suspensions using NaOH, Na<sub>2</sub>CO<sub>3</sub>, Na<sub>2</sub>C<sub>2</sub>O<sub>4</sub> and Na<sub>4</sub>P<sub>2</sub>O<sub>7</sub> are presented in Fig. 3, and other elements are provided in Fig. S1. These elements were selected because they illustrate the effect of extractants on the different NNM phases. Overall, elemental concentrations increased following the order: NaOH  $\approx$  Na<sub>2</sub>CO<sub>3</sub>  $\leq$  Na<sub>2</sub>C<sub>2</sub>O<sub>4</sub> < Na<sub>4</sub>P<sub>2</sub>O<sub>7</sub>. This trend follows the same trend of SOM concentration (inferred from UV–Vis absorbance, Fig. 1) in NNM suspensions indicating the co-release of NNMs and SOM from soil microaggregates. For Na<sub>2</sub>C<sub>2</sub>O<sub>4</sub> and Na<sub>2</sub>CO<sub>3</sub> extracted NNMs, the elemental concentrations did not follow a clear trend with the increase in pH or extractant concentration (Fig. 3). For Na<sub>4</sub>P<sub>2</sub>O<sub>7</sub> extracted NNMs, elemental concentrations were generally higher (2 to 12

folds) than those measured in NaOH extracted NNM suspensions (Fig. 3). Elemental concentrations generally increased with the increase in solution pH at 2 and 10 mM Na<sub>4</sub>P<sub>2</sub>O<sub>7</sub>. The element extraction pH-dependency can be attribute to the pyrophosphate speciation with higher proportion of  $P_2O_7^{4-}$  (e.g., <5% at pH 8 vs 50% at pH 10) in comparison to  $HP_2O_7^{3-}$  at higher pH values (Masala et al., 2002). However, elemental concentrations did not change or even decreased with the increase in pH at 100 mM Na<sub>4</sub>P<sub>2</sub>O<sub>7</sub>. The increase in elemental concentrations with the increase in Na<sub>4</sub>P<sub>2</sub>O<sub>7</sub> concentration was element-specific. Cerium concentration (Fig. 3a) increased by 8 folds with the increase in Na<sub>4</sub>P<sub>2</sub>O<sub>7</sub> concentration from 2 to 100 mM, whereas Al, Ti and V concentrations increased slightly by 1.4 to 1.8 folds with the increase in Na<sub>4</sub>P<sub>2</sub>O<sub>7</sub> concentration. These differences may be attributed to the affinity of these elements to Na<sub>4</sub>P<sub>2</sub>O<sub>7</sub>, suggesting that Na<sub>4</sub>P<sub>2</sub>O<sub>7</sub> results in selective extraction of Ce phases, and/or that Al, Ti and V occur dominantly in larger particles.

These results suggest that the increase in NNM surface charge by increasing suspension pH using indifferent electrolyte is insufficient to significantly disperse NNMs from soil microaggregates which is supported by nearly-constant elemental concentrations for NaOH extracted NNMs at pH 8, 9 and 10. Chemical extractants (i.e., Na<sub>4</sub>P<sub>2</sub>O<sub>7</sub> and Na<sub>2</sub>C<sub>2</sub>O<sub>4</sub>) enhance NNM dispersion from soil microaggregates *via* several mechanisms (depicted in Fig. 4) including (i) complexation of multivalent cations (Mekmene and Gaucheron, 2011), (ii) specific sorption on NNM surfaces resulting in displacement of SOM from NNM surfaces (Arai and Sparks, 2001; Connor and McQuillan, 1999; Regelink et al., 2013b), and enhancement of NNM ζ potential (Pham et al., 2014). Complexation of multivalent cations reduces the concentration of free multivalent cations in solution, and thus reduces NNM aggregation via surface charge screening and or bridging mechanism (Chen et al., 2006, 2007). Combined, these mechanisms result in an overall increase in the release of SOM and NNM from soil microaggregates as demonstrated for Na<sub>4</sub>P<sub>2</sub>O<sub>7</sub> and Na<sub>2</sub>C<sub>2</sub>O<sub>4</sub> extractions (Arai and Sparks, 2001; He et al., 1999; Regelink et al., 2013b). However, the release of polyvalent cations (e.g.,  $Ca^{2+}$ ,  $Al^3$ <sup>+</sup>, Fe<sup>3+</sup>, Mg<sup>2+</sup>) from soil microaggregates during the extraction process may result in NNM heteroaggregation via NNM-SOM bridging mechanism (Zhou et al., 2012). The higher efficiency of Na<sub>4</sub>P<sub>2</sub>O<sub>7</sub> compared to Na<sub>2</sub>C<sub>2</sub>O<sub>4</sub> can be attributed to the higher affinity of Na<sub>4</sub>P<sub>2</sub>O<sub>7</sub> to multivalent cations (e.g.,  $K_{ap}$  for  $Ca^{2+}$  of  $10^5$  and  $10^3$   $M^{-1}$ , respectively) (Furia, 1972) and NNM surfaces (Burlamacchi et al., 1983; Doetterl et al., 2015).

#### 3.3. Effect of extraction conditions on NNM size distribution by AF4-ICP-MS

#### 3.3.1. Effect of extractant at constant concentration and pH

The elemental size distributions of Al, Ti, V and Ce containing NNMs extracted using NaOH, Na<sub>4</sub>P<sub>2</sub>O<sub>7</sub>, Na<sub>2</sub>C<sub>2</sub>O<sub>4</sub> and Na<sub>2</sub>CO<sub>3</sub> at pH 10 and 10 mM concentration are presented in Fig. 5. For all elements except Al, NNM concentration increased following the order: NaOH ~ Na<sub>2</sub>CO<sub>3</sub> < Na<sub>2</sub>C<sub>2</sub>O<sub>4</sub> < Na<sub>4</sub>P<sub>2</sub>O<sub>7</sub>, in good agreement with the total elemental concentrations measured following total NNM digestion (Fig. 3). Na<sub>4</sub>P<sub>2</sub>O<sub>7</sub> extracted NNMs are characterized by the highest elemental concentrations (ca. 2–5 folds higher than NaOH extracted NNMs), the narrowest size distribution, and the smallest modal hydrodynamic diameter. These findings suggest that Na<sub>4</sub>P<sub>2</sub>O<sub>7</sub> extraction results in the release of metal-containing NNMs from soil microaggregates as small aggregates and/or primary NNMs. These observations were further corroborated by TEM analysis of NaOH and Na<sub>4</sub>P<sub>2</sub>O<sub>7</sub> extracted NNMs (Fig. 6). NaOH extracted NNMs occur mostly as heteroaggregates of NNMs with larger particles (Fig. 6a), whereas Na<sub>4</sub>P<sub>2</sub>O<sub>7</sub> extracted NNMs occur mostly as dispersed primary particles and small aggregates (Fig. 6b).

# 3.3.2. Effect of Na<sub>4</sub>P<sub>2</sub>O<sub>7</sub> and Na<sub>2</sub>CO<sub>3</sub> concentration at constant pH

The elemental size distributions of Al, Ti, V and Ce rich NNMs extracted using 2, 10 and 100 mM  $Na_2CO_3$  and  $Na_4P_2O_7$  at pH 10 are presented in Fig. 7. For  $Na_4P_2O_7$  extracted NNMs, the elemental size

distributions and the modal hydrodynamic diameter shift toward smaller sizes with the increase in Na<sub>4</sub>P<sub>2</sub>O<sub>7</sub> concentration (Fig. 7a-d). For Na<sub>2</sub>CO<sub>3</sub> extracted NNMs, NNM size distribution was not significantly impacted by Na<sub>2</sub>CO<sub>3</sub> concentrations. However, the elemental concentration decreased with the increase in Na<sub>2</sub>CO<sub>3</sub> concentration (Fig. 7eh), likely due to NNM aggregation. This hypothesis is supported by the increased in NNM hydrodynamic diameter measured by DLS (Fig. 2a) and the decrease in NNM  $\zeta$  potential magnitude with the increase in  $Na_2CO_3$  concentration (e.g., from  $-33.7 \pm 0.9$  and  $-35.5 \pm 2.1$  at 2 and 10 mM to  $-28.5 \pm 2.5$  at 100 mM, Table S2). For Na<sub>2</sub>CO<sub>3</sub> extracted NNMs, titanium was not detected by AF4-ICP-MS and the concentrations of Ce, and V bearing NNMs were very low at all pHs, indicating that Na<sub>2</sub>CO<sub>3</sub> is not suitable for the extraction of these NNMs. For a given element at constant extractant concentration, Na<sub>4</sub>P<sub>2</sub>O<sub>7</sub> extracted NNMs exhibited narrower size distribution, smaller modal hydrodynamic diameter, and higher concentrations (1.5 to 5 folds) relative to Na<sub>2</sub>CO<sub>3</sub> extracted NNMs. Thus, Na<sub>4</sub>P<sub>2</sub>O<sub>7</sub> is more suitable than Na<sub>2</sub>CO<sub>3</sub> to extract NNMs from soils.

#### 3.3.3. Effect of pH at 10 and 100 mM $Na_4P_2O_7$

The elemental size distributions of Al, Ti, V and Ce bearing NNMs extracted using 10 mM and 100  $Na_4P_2O_7$  at pH 8, 9 and 10 are presented in Fig. 8. At 10 mM  $Na_4P_2O_7$ , the concentration of the extracted NNMs increases up to 5 folds with the increase in pH from 8 to 10. NNM  $\zeta$  potential

magnitude increases with pH from 8 to 10 (Table S2), resulting in larger repulsive forces between NNMs, which may enhance the release of NNMs from soil microaggregates. All elements, except Al, show similar size distributions at the different pHs. Al-containing NNMs exhibited broader size distributions with the increase in pH indicating the extraction of larger Al-containing NNMs with the increase in pH. At 100 mM  $\rm Na_4P_2O_7$ , the elemental size distribution of all elements remained the same with the increase in pH. The concentration of Al, Ti, and V-containing NNMs remained constant with the increase in pH, whereas the concentration of and Ce-containing NNMs increase with the increase in pH. This increase in Ce concentration with the increase in pH can be attributed to the specific interaction of pyrophosphate Ce rich NNMs.

#### 3.4. Elemental association and ratios

The elemental ratios of Zr to Hf, Ti to Nb, Ti to Ta, and Ce to La were relatively constant under all extraction conditions (Fig. 9) indicating strong association between these elements, likely within the same mineral phase. Nonetheless, elemental ratios calculated from total elemental concentrations do not exclusively indicate the association between these elements with the same particle/phase, could be biased by dissolved ions in the solution, and vary with particle size. Size based-elemental ratios obtained by AF4-ICP-MS analysis are intrinsic to NNMs as dissolved ions pass through the AF4 accumulation wall and

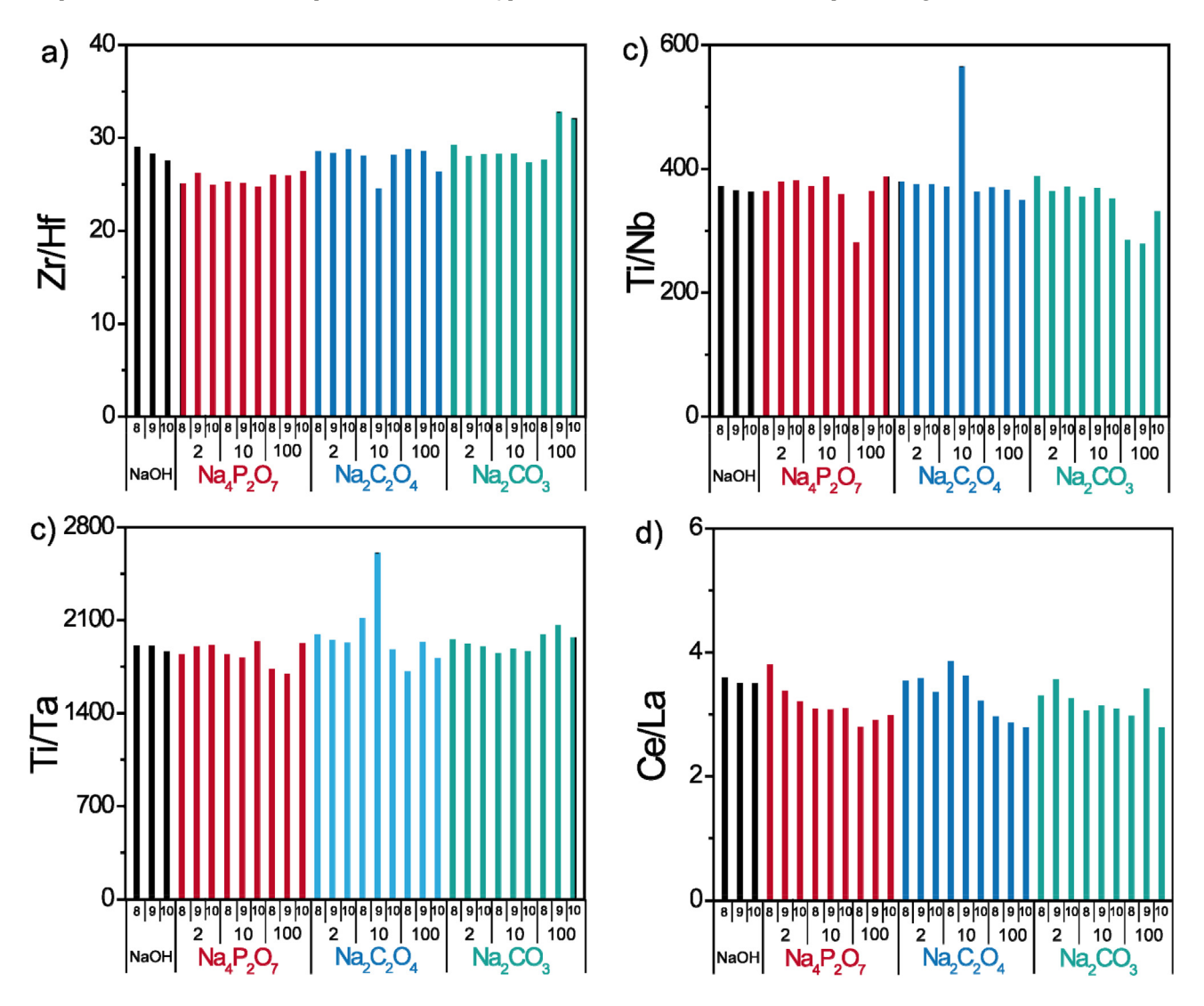


Fig. 9. Elemental ratios of total digested soil nanosize fraction extracted by different dispersing agents at different concentration and pH conditions. In the x-axis title, the top numbers represent the pH and the second number represents the concentration of the chemical dispersants.

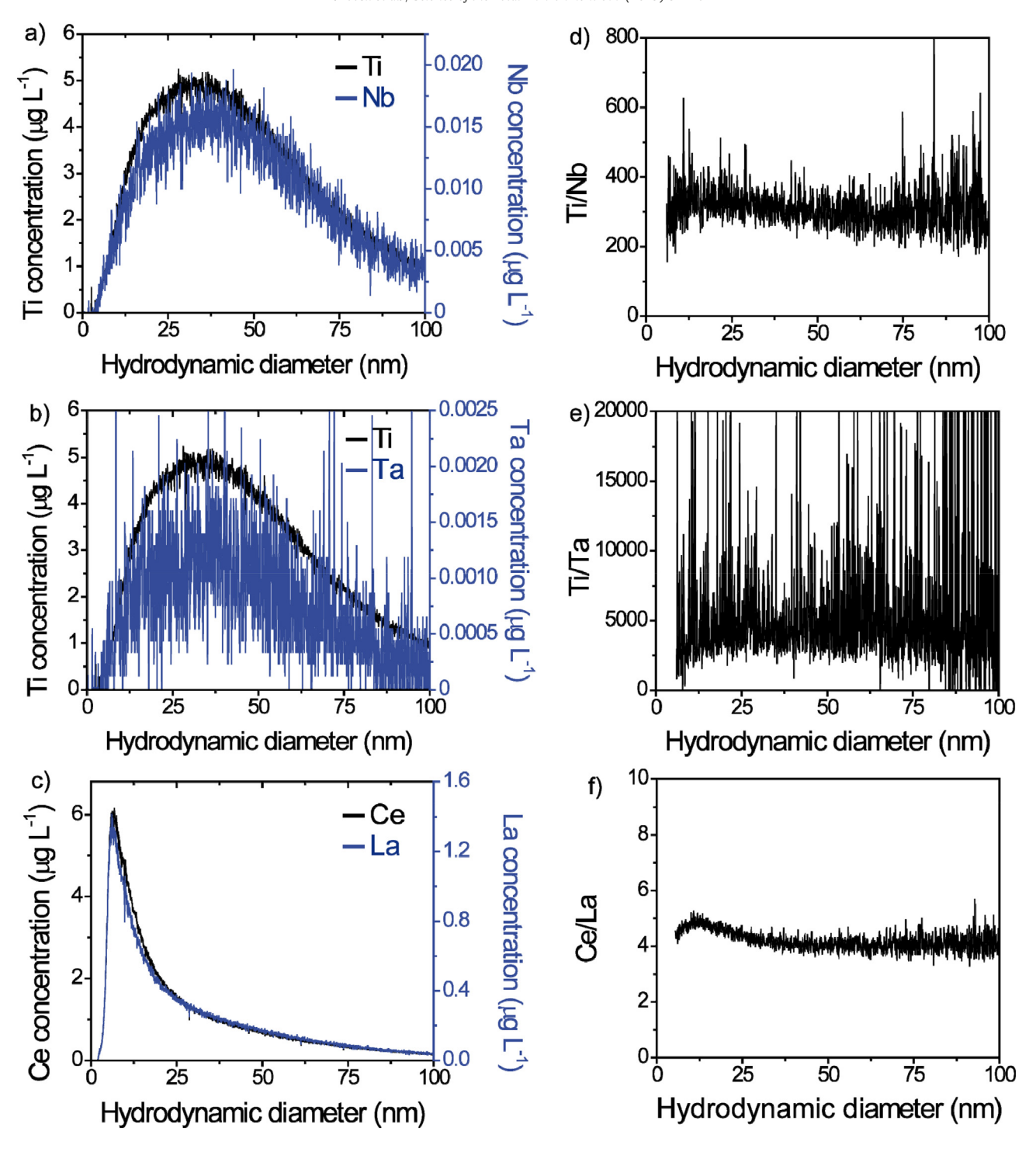


Fig. 10. Elemental size distributions of (a) Ti and Nb (b) Ti and Ta, (c) Ce and La, and the (d, e, and f) the corresponding size-based elemental ratios. NNMs were extracted with 10 mM  $Na_4P_2O_7$  at pH 10.

only NNMs are analyzed by ICP-MS. Fig. 10a and b show that Ti, Nb and Ta co-elute at the same elution time/hydrodynamic diameter and Fig. 10c show that Ce and La co-elute at the same elution time/hydrodynamic diameter. The elemental ratio of Ti to Nb was constant at approximately 300 for all NNM sizes in good agreement with elemental ratio calculated from the total elemental concentrations (Fig. 9b) and with the average crustal Ti to Nb elemental ratio of 312 (Wedepohl, 1995). Similarly, the elemental ratio of Ti to Ta was constant at approximately 2000 for all NNM sizes, in good agreement with elemental ratio calculated from the total elemental concentrations (Fig. 9c) and the average crustal Ti to Ta elemental ratio (Wedepohl, 1995). Overall, these results

indicate strong association between Ti, Nb and Ta in soil NNM independent of the particle size. Given the higher Nb content in NNMs (e.g., smaller Ti/Nb ratio), Nb is most likely to provide more accurate results when determining shift in elemental ratios, in particular for AF4-ICP-MS analysis to avoid high volume injections in order to detect Ta. Ce/La ratio is also nearly constant as a function of particle size at approximately 4 (Fig. 10f) in good agreement with elemental ratio calculated from the total elemental concentrations (Fig. 9b) and with the average crustal Ti to Nb elemental ratio. Thus, the elemental ratio of Ce to La can also be used as good proxy for the detection of cerium oxide ENM in soils (Montano et al., 2014; Navratilova et al., 2015). These elemental

associations can be used to track NM sources (*e.g.*, natural or engineered) by monitoring the increase in these elemental ratios due to contamination with pure ENMs (Gondikas et al., 2018; Loosli et al., 2019).

#### 4. Conclusion

Extraction of NNMs from soils is vital to facilitate NNM characterization, to better understand elemental associations and ratios within NNMs, and to develop approaches to differentiate engineered from natural particles. This study investigated systematically the effect of extractant composition, concentration, and pH on the extraction efficiency and properties of soil NNMs. Na<sub>4</sub>P<sub>2</sub>O<sub>7</sub> at a concentration of 10 mM and pH 9-10 extracted the highest concentrations of NNMs. Although, Na<sub>2</sub>C<sub>2</sub>O<sub>4</sub>, and to a lesser extend Na<sub>2</sub>CO<sub>3</sub>, generally extracted higher concentrations of NNMs in comparison to NaOH, the NNMs were extracted in the form of small aggregates of multiple primary NNMs. The extracted NNMs were characterized by constant, and size-independent, elemental ratios of Ti to Nb, Ti to Ta, and Ce to La, and these ratios were in close proximity to those calculated based on the average crustal elemental composition. This study presents a comprehensive approach to characterize soil NNMs based on dispersion and extraction of NNMs, total metal concentration, size fractionation and detection by AF4-ICP-MS, and microscopic analysis. Future studies will focus on determining the elemental associations and ratios in NNMs extracted from different geological formation and geographic locations to further support the implementation of these elemental associations and ratios to distinguish natural from engineered particles globally.

#### Acknowledgment

This work was supported by US National Science Foundation CAREER (1553909) grant to Dr. Mohammed Baalousha, Swiss National Science Foundation postdoctoral mobility funding (P2GEP2\_165046) to Dr. Frédéric Loosli and China Scholarship Council (CSC\_201606380069) grant to Dr. Zebang Yi. This work was also supported by the Virginia Tech National Center for Earth and Environmental Nanotechnology Infrastructure (NanoEarth), a member of the National Nanotechnology Coordinated Infrastructure (NNCI), supported by NSF (ECCS 1542100).

# Appendix A. Supplementary data

Supplementary data to this article can be found online at https://doi.org/10.1016/j.scitotenv.2019.04.301.

#### References

- Albrektienė, R., Rimeika, M., Zalieckienė, E., Šaulys, V., Zagorskis, A., 2012. Determination of organic matter by UV absorption in the ground water. J. Environ. Eng. Landsc. Manag. 20 (2), 163–167.
- Arai, Y., Sparks, D.L., 2001. ATR-FTIR spectroscopic investigation on phosphate adsorption mechanisms at the ferrihydrite-water interface. J. Colloid Interface Sci. 241 (2), 317–326.
- Baalousha, M., 2009. Aggregation and disaggregation of iron oxide nanoparticles: influence of particle concentration, pH and natural organic matter. Sci. Total Environ. 407 (6), 2093–2101.
- Baalousha, M., Lead, J.R., 2012. Rationalizing nanomaterial sizes measured by atomic force microscopy, flow field-flow fractionation, and dynamic light scattering: sample preparation, polydispersity, and particle structure. Environ. Sci. Technol. 46 (11), 6134–6142.
- Baalousha, M., Kammer, F.V.D., Motelica-Heino, M., Le Coustumer, P., 2005. 3D characterization of natural colloids by FIFFF-MALLS-TEM. Anal. Bioanal. Chem. 383 (4), 549–556
- Bakshi, S., He, Z.L., Harris, W.G., 2014. A new method for separation, characterization, and quantification of natural nanoparticles from soils. J. Nanopart. Res. 16 (2).
- Buchanan, W., Roddick, F., Porter, N., Drikas, M., 2005. Fractionation of UV and VUV pretreated natural organic matter from drinking water. Environ. Sci. Technol. 39 (12), 4647–4654.

- Buffle, J., Wilkinson, K.J., Stoll, S., Filella, M., Zhang, J.W., 1998. A generalized description of aquatic colloidal interactions: the three-colloidal component approach. Environ. Sci. Technol. 32 (19), 2887–2899.
- Burlamacchi, L., Lai, A., Monduzzi, M., 1983. Adsorption of aluminium and pyrophosphate ions at a TiO2 surface studied by 27Al and 31 P NMR spectroscopy. Chem. Phys. Lett. 100 (6). 549–552.
- Calabi-Floody, M., Bendall, J.S., Jara, A.A., Welland, M.E., Theng, B.K.G., Rumpel, C., Mora, M. d.I.L., 2011. Nanoclays from an Andisol: Extraction, properties and carbon stabilization. Geoderma 161 (3), 159–167.
- Chen, X., Mao, S.S., 2007. Titanium dioxide nanomaterials: synthesis, properties, modifications, and applications. Chem. Rev. 107 (7), 2891–2959.
- Chen, K.L., Mylon, S.E., Elimelech, M., 2006. Aggregation kinetics of alginate-coated hematite nanoparticles in monovalent and divalent electrolytes. Environ. Sci. Technol. 40 (5), 1516–1523.
- Chen, K.L., Mylon, S.E., Elimelech, M., 2007. Enhanced aggregation of alginate-coated Iron oxide (hematite) nanoparticles in the presence of calcium, strontium, and barium cations. Langmuir 23 (11), 5920–5928.
- Connor, P.A., McQuillan, A.J., 1999. Phosphate adsorption onto TiO2 from aqueous solutions: an in situ internal reflection infrared spectroscopic study. Langmuir 15 (8), 2916–2921.
- Cornelis, G., Hund-Rinke, K., Kuhlbusch, T., van den Brink, N., Nickel, C., 2014. Fate and bioavailability of engineered nanoparticles in soils: a review. Crit. Rev. Environ. Sci. Technol. 44 (24), 2720–2764.
- von der Kammer, F., Ferguson, P.L., Holden, P.A., Masion, A., Rogers, K.R., Klaine, S.J., Koelmans, A.A., Horne, N., Unrine, J.M., 2012. Analysis of engineered nanomaterials in complex matrices (environment and biota): general considerations and conceptual case studies. Environ. Toxicol. Chem. 31 (1), 32–49.
- Doetterl, S., Cornelis, J.T., Six, J., Bode, S., Opfergelt, S., Boeckx, P., Van Oost, K., 2015. Soil redistribution and weathering controlling the fate of geochemical and physical carbon stabilization mechanisms in soils of an eroding landscape. Biogeosciences 12 (5), 1357–1371.
- El Hadri, H., Louie, S.M., Hackley, V.A., 2018. Assessing the interactions of metal nanoparticles in soil and sediment matrices a quantitative analytical multi-technique approach. Environ. Sci. Nano 5 (1), 203–214.
- Fisher-Power, L.M., Cheng, T., 2018. Nanoscale titanium dioxide (nTiO2) transport in natural sediments: importance of soil organic matter and Fe/Al oxyhydroxides. Environ. Sci. Technol. 52 (5). 2668–2676.
- Furia, T.E., 1972. CRC Handbook of Food Additives. CRC Press, Cleveland.
- Gieseking, J.E., 1975a. Soil Components Volume 1: Organic Components. Springer-Verlag, Berlin Heidelberg.
- Gieseking, J.E., 1975b. Soil Components Volume 2: Inorganic Components. Springer-Verlag, Berlin Heidelberg.
- Gondikas, A., von der Kammer, F., Kaegi, R., Borovinskaya, O., Neubauer, E., Navratilova, J., Praetorius, A., Cornelis, G., Hofmann, T., 2018. Where is the nano? Analytical approaches for the detection and quantification of TiO2 engineered nanoparticles in surface waters. Environ. Sci. Nano 5 (2), 313–326.
- He, J.Z., De Cristofaro, A., Violante, A., 1999. Comparison of adsorption of phosphate, tartrate, and oxalate on hydroxy aluminum montmorillonite complexes. Clay Clay Miner. 47 (2), 226–233.
- Jeanroy, E., Guillet, B., 1981. The occurrence of suspended ferruginous particles in pyrophosphate extracts of some soil horizons. Geoderma 26 (1–2), 95–105.
- Jiang, J.K., Oberdorster, G., Biswas, P., 2009. Characterization of size, surface charge, and agglomeration state of nanoparticle dispersions for toxicological studies. I. Nanopart. Res. 11 (1), 77–89.
- Jolivet, J.P., 2000. Metal Oxide Chemistry and Synthesis: From Solution to Solid State.
- Keller, A.A., Lazareva, A., 2014. Predicted releases of engineered nanomaterials: from global to regional to local. Environ. Sci. Technol. Lett. 1 (1), 65–70.
- Klaine, S.J., Alvarez, P.J.J., Batley, G.E., Fernandes, T.F., Handy, R.D., Lyon, D.Y., Mahendra, S., McLaughlin, M.J., Lead, J.R., 2008. Nanomaterials in the environment: behavior, fate, bioavailability, and effects. Environ. Toxicol. Chem. 27 (9), 1825–1851.
- Li, W., He, Y., Wu, J., Xu, J., 2012. Extraction and characterization of natural soil nanoparticles from Chinese soils. Eur. J. Soil Sci. 63 (5), 754–761.
- Liu, J.B., Hwang, Y.S., Lenhart, J.J., 2015. Heteroaggregation of bare silver nanoparticles with clay minerals. Environ. Sci. Nano 2 (5), 528–540.
- Loosli, F., Le Coustumer, P., Stoll, S., 2015. Effect of electrolyte valency, alginate concentration and pH on engineered TiO2 nanoparticle stability in aqueous solution. Sci. Total Environ. 535, 28–34.
- Loosli, F., Yi, Z., Berti, D., Baalousha, M., 2018. Toward a better extraction of titanium dioxide engineered nanomaterials from complex environmental matrices. NanoImpact 11, 119–127.
- Loosli, F., Wang, J., Rothenberg, S., Bizimis, M., Winkler, C., Borovinskaya, O., Flamigni, L., Baalousha, M., 2019. Sewage spills are a major source of titanium dioxide engineered (nano)-particle release into the environment. Environ. Sci. Nano 6 (3), 763–777.
- Lu, A.-H., Salabas, E.L., Schueth, F., 2007. Magnetic nanoparticles: synthesis, protection, functionalization, and application. Angew. Chem. Int. Ed. 46 (8), 1222–1244.
- Makino, K., Ohshima, H., 2010. Electrophoretic mobility of a colloidal particle with constant surface charge density. Langmuir 26 (23), 18016–18019.
- Masala, O., McInnes, E.J.L., O'Brien, P., 2002. Modelling the formation of granules: the influence of manganese ions on calcium pyrophosphate precipitates. Inorg. Chim. Acta 339, 366–372.
- McCarthy, J.F., Zachara, J.M., 1989. Subsurface transport of contaminants mobile colloids in the subsurface environment may alter the transport of contaminants. Environ. Sci. Technol. 23 (5), 496–502.
- Mekmene, O., Gaucheron, F., 2011. Determination of calcium-binding constants of caseins, phosphoserine, citrate and pyrophosphate: a modelling approach using free calcium measurement. Food Chem. 127 (2), 676–682.

- Montano, M.D., Lowry, G.V., von der Kammer, F., Blue, J., Ranville, J.F., 2014. Current status and future direction for examining engineered nanoparticles in natural systems. Environ. Chem. 11 (4), 351–366.
- Mueller, N.C., Nowack, B., 2008. Exposure modeling of engineered nanoparticles in the environment. Environ. Sci. Technol. 42 (12), 4447–4453.

  Murdock, R.C., Braydich-Stolle, L., Schrand, A.M., Schlager, J.J., Hussain, S.M., 2007. Charac-
- Murdock, R.C., Braydich-Stolle, L., Schrand, A.M., Schlager, J.J., Hussain, S.M., 2007. Characterization of nanomaterial dispersion in solution prior to in vitro exposure using dynamic light scattering technique. Toxicol. Sci. 101 (2), 239–253.
- Navratilova, J., Praetorius, A., Gondikas, A., Fabienke, W., von der Kammer, F., Hofmann, T., 2015. Detection of engineered copper nanoparticles in soil using single particle ICP-MS. Int. I. Environ. Res. Public Health 12 (12), 15756–15768.
- Novikova, L., Ayrault, P., Fontaine, C., Chatel, G., Jérôme, F., Belchinskaya, L., 2016. Effect of low frequency ultrasound on the surface properties of natural aluminosilicates. Ultrason. Sonochem. 31, 598–609.
- Nowack, B., Bucheli, T.D., 2007. Occurrence, behavior and effects of nanoparticles in the environment. Environ. Pollut. 150 (1), 5–22.
- Pham, D.V., Ishiguro, M., Tran, H.T.T., Sato, T., 2014. Influence of phosphate sorption on dispersion of a ferralsol. Soil Sci. Plant Nutr. 60 (3), 356–366.
- Philippe, A., Schaumann, G.E., 2014. Interactions of dissolved organic matter with natural and engineered inorganic colloids: a review. Environ. Sci. Technol. 48 (16), 8946–8962.
- Piccinno, F., Gottschalk, F., Seeger, S., Nowack, B., 2012. Industrial production quantities and uses of ten engineered nanomaterials in Europe and the world. J. Nanopart. Res. 14 (9), 1109.
- Praetorius, A., Gundlach-Graham, A., Goldberg, E., Fabienke, W., Navratilova, J., Gondikas, A., Kaegi, R., Günther, D., Hofmann, T., von der Kammer, F., 2017. Single-particle multi-element fingerprinting (spMEF) using inductively-coupled plasma time-of-flight mass spectrometry (ICP-TOFMS) to identify engineered nanoparticles against the elevated natural background in soils. Environ. Sci.: Nano 4 (2), 307–314.
- Praetorius, A., Labille, J., Scheringer, M., Thill, A., Hungerbuhler, K., Bottero, J.Y., 2014. Heteroaggregation of titanium dioxide nanoparticles with model natural colloids under environmentally relevant conditions. Environ. Sci. Technol. 48 (18), 10690–10698.
- Prasad, A., Baalousha, M., Lead, J.R., 2015. An electron microscopy based method for the detection and quantification of nanomaterial number concentration in environmentally relevant media. Sci. Tot. Environ. 537, 479–486.
- Pronk, G.J., Heister, K., Kogel-Knabner, I., 2011. Iron oxides as major available Interface component in loamy arable topsoils. Soil Sci. Soc. Am. J. 75 (6), 2158–2168.

- Regelink, I.C., Koopmans, G.F., van der Salm, C., Weng, L.P., van Riemsdijk, W.H., 2013a. Characterization of colloidal phosphorus species in drainage waters from a clay soil using asymmetric flow field-flow fractionation. J. Environ. Qual. 42 (2), 464–473.
- Regelink, I.C., Weng, L., Koopmans, G.F., Van Riemsdijk, W.H., 2013b. Asymmetric flow field-flow fractionation as a new approach to analyse iron-(hydr)oxide nanoparticles in soil extracts. Geoderma 202. 134–141.
- Shamrikova, E.V., Ryazanov, M.A., Vanchikova, E.V., 2006. Acid-base properties of water-soluble organic matter of forest soils, studied by the pK-spectroscopy method. Chemosphere 65 (8), 1426–1431.
- Shamrikova, E.V., Vanchikova, E.V., Ryazanov, M.A., 2007. Study of the acid-base properties of mineral soil horizons using pK spectroscopy. Eurasian Soil Sci. 40 (11), 1169–1174
- Song, R., Qin, Y., Suh, S., Keller, A.A., 2017. Dynamic model for the stocks and release flows of engineered nanomaterials. Environ. Sci. Technol. 51 (21), 12424–12433.
- Stark, W.J., Stoessel, P.R., Wohlleben, W., Hafner, A., 2015. Industrial applications of nanoparticles. Chem. Soc. Rev. 44 (16), 5793–5805.
- Suttiponparnit, K., Jingkun, J., Sahu, M., Suvachittanont, S., Charinpanitkul, T., Biswas, P., 2011. Role of surface area, primary particle size, and crystal phase on titanium dioxide nanoparticle dispersion properties. Nano Scale Res. Lett. 6 (1), 27 (28 pp.)-27 (28 pp.).
- Tang, Z.Y., Wu, L.H., Luo, Y.M., Christie, P., 2009. Size fractionation and characterization of nanocolloidal particles in soils. Environ. Geochem. Health 31 (1), 1–10.
- Theng, B.K.G., Yuan, G., 2008. Nanoparticles in the soil environment. Elements 4 (6), 395–399.
- USDA, 2017. Dothan Series.
- Wagner, S., Gondikas, A., Neubauer, E., Hofmann, T., von der Kammer, F., 2014. Spot the difference: engineered and natural nanoparticles in the environment-release, behavior, and fate. Angew. Chem. Int. Ed. 53 (46), 12398–12419.
- Wang, H.T., Adeleye, A.S., Huang, Y.X., Li, F.T., Keller, A.A., 2015. Heteroaggregation of nanoparticles with biocolloids and geocolloids. Adv. Colloid Interf. Sci. 226, 24–36.
- Wedepohl, K., 1995. The composition of the continental crust. Geochim. Cosmochim. Acta 59 (7), 1217–1232.
- Zhou, D., Abdel-Fattah, A.I., Keller, A.A., 2012. Clay particles destabilize engineered nanoparticles in aqueous environments. Environ. Sci. Technol. 46 (14), 7520–7526.